



# Computational Fluid Dynamics Modeling of a 40-mm Grenade With and Without Jet Flow

by Jubaraj Sahu and Karen R. Heavey

ARL-TR-2572

September 2001

Approved for public release; distribution is unlimited.

20011005 373

The findings in this report are not to be construed as an official Department of the Army position unless so designated by other authorized documents.

Citation of manufacturer's or trade names does not constitute an official endorsement or approval of the use thereof.

Destroy this report when it is no longer needed. Do not return it to the originator.

# Army Research Laboratory

Aberdeen Proving Ground, MD 21005-5066

---

ARL-TR-2572

September 2001

---

## Computational Fluid Dynamics Modeling of a 40-mm Grenade With and Without Jet Flow

Jubaraj Sahu and Karen R. Heavey  
Weapons and Materials Research Directorate, ARL

---

Approved for public release; distribution is unlimited.

---

---

## Abstract

---

This report describes a computational study undertaken to consider the aerodynamic effect of small tiny jets as a means to provide the control authority needed to maneuver a projectile at low subsonic speeds. Scalable Navier-Stokes computational techniques have been used to obtain numerical solutions for the jet-interaction flow field for a projectile at subsonic speeds. Computed results have been obtained at low subsonic speeds at  $0^\circ$  and  $4^\circ$  angle of attack. Both steady and unsteady jets have been considered. For comparison purposes, a jet-off case was also computed. Qualitative flow field features show the interaction of jets with the free stream flow. Numerical results show the effect of the jet locations and sizes on the flow field and surface pressures, and hence on the aerodynamic coefficients. Unsteady jet results have been obtained for a two-dimensional (2-D) jet flow and compared with experimental data for validation. Some results obtained with an unsteady jet for the subsonic projectile are included. These numerical results are being assessed to determine if small tiny jets can be used to provide the control authority needed for maneuvering munitions in lieu of canards and fins.

---

## Contents

---

List of Figures	v
List of Tables	vii
1. Introduction	1
2. Solution Technique	2
2.1 Governing Equations.....	2
2.2 Numerical Algorithm .....	3
2.3 Boundary Conditions.....	4
3. Chimera Composite Grid Scheme	4
4. Model Geometry and Computational Grid	5
5. Results	8
5.1 Jet-Off.....	8
5.2 Steady Jet .....	11
5.3 Unsteady Jet .....	13
6. Conclusion	20
7. References	21
Distribution List	23
Report Documentation Page	27

INTENTIONALLY LEFT BLANK.

---

## List of Figures

---

Figure 1. Model of the 40-mm grenade. ....	2
Figure 2. Computational model and grid system. ....	6
Figure 3. Location of nose jets on the computational model. ....	6
Figure 4. Location of cylinder jets on the computational model. ....	7
Figure 5. Computational model showing jet cavity. ....	7
Figure 6. Convergence history, jet-off. ....	8
Figure 7. Pressure contours, jet-off; Mach numbers 0.15, 0.2, and 0.25 (top to bottom). ....	9
Figure 8. Mach number vs. drag coefficients, jet-off. ....	10
Figure 9. Velocity vectors, base region, jet-off. ....	10
Figure 10. Surface pressure coefficient vs. axial position. ....	12
Figure 11. Drag coefficient vs. axial position. ....	12
Figure 12. Pressure contours in nose area, (a) jet-off and (b) jet-on. ....	13
Figure 13. Pressure contours in cylinder area, (a) jet-off and (b) jet-on. ....	13
Figure 14. Surface pressure coefficient – nose jets. ....	14
Figure 15. Surface pressure coefficient – cylinder jets. ....	14
Figure 16. Surface pressure contours – cylinder jets. ....	15
Figure 17. Pressure contours, cylinder jets, longitudinal view. ....	15
Figure 18. Schematic and flow picture of a 2-D jet experiment. ....	16
Figure 19. Velocity components $u$ , $v$ , and vorticity for an unsteady jet. ....	17
Figure 20. Variation of time-averaged centerline jet velocity with distance from the wall, unsteady jet. ....	17
Figure 21. Computed surface pressures, $M = 0.25$ , $\alpha = 0$ , unsteady jet. ....	18
Figure 22. Velocity vectors at two instants in time during the cycle, $M = 0.25$ , $\alpha = 0$ , unsteady jet. ....	19
Figure 23. Force and moment coefficients, $M = 0.25$ , $\alpha = 0$ , unsteady jet. ....	19
Figure 24. Force and moment coefficients, $M = 0.25$ , $\alpha = 0$ , unsteady jet. ....	20

INTENTIONALLY LEFT BLANK.

---

## List of Tables

---

Table 1. Force and moment coefficients for nose jets, $\alpha = 4$ . .....	16
Table 2. Force and moment coefficients for cylinder jets, $\alpha = 4$ . .....	16

INTENTIONALLY LEFT BLANK.

---

## 1. Introduction

---

The prediction of aerodynamic coefficients for projectile configurations is essential in assessing the performance of new designs. Accurate determination of aerodynamics is critical to the low-cost development of new advanced guided projectiles, rockets, missiles, and smart munitions. Fins, canards, and jets can be used to provide control for maneuvering projectiles and missiles. The flow fields associated with these control mechanisms for U.S. Army weapons are complex involving three-dimensional (3-D) shock-boundary layer interactions, jet-interaction with the free stream flow, and highly viscous-dominated separated flow regions. The jet interference extends over significant portions of the projectile and must be modeled correctly. For missiles, jet thrusters have been studied over a number of years to provide high-speed aerodynamic control. These thrusters interact with the surrounding flow field; again, the resulting jet interaction flow field is complex. Recently, several studies have shown that small tiny microelectromechanical system (MEMS) jets can significantly alter the flow field and pressure distributions for airfoils and cylinders. The present analysis involves the use of these tiny jets for projectile aerodynamic control. The emphasis in the present research is to provide insight into the interaction of these jets with the free stream flow and to determine the feasibility of these jets for aerodynamic control of a subsonic projectile. Both computational and experimental data for these jet interactions are very limited. Simple theories cannot predict the complex flow fields associated with the jet interaction and experimental tests are very expensive. To help reduce experimental costs, computational fluid dynamics (CFD) is being used to predict these complex flows and to provide detailed pressure and force and moment data. The advanced CFD capability used here solves the Navier-Stokes equations and incorporates the Chimera technique. This numerical capability has been used successfully to determine the aerodynamics on a number of complex military systems [1-3] of interest to the U.S. Army.

This report describes the application of CFD to a 40-mm grenade with MEMS jets. Figure 1 shows a model of this projectile. The problem involves 3-D flow computations on a medium-caliber subsonic grenade with multiple jet holes. However, the scope of this report is limited to a single jet hole. By varying the size of the jet hole as well as its location on the projectile body, a range of computational results has been provided. Numerical flow field computations have been made for both steady and unsteady jets at a low subsonic speed. The unsteady jet case for this subsonic projectile includes modeling the inside of the jet cavity. The purpose is to determine the resulting aerodynamic forces on the

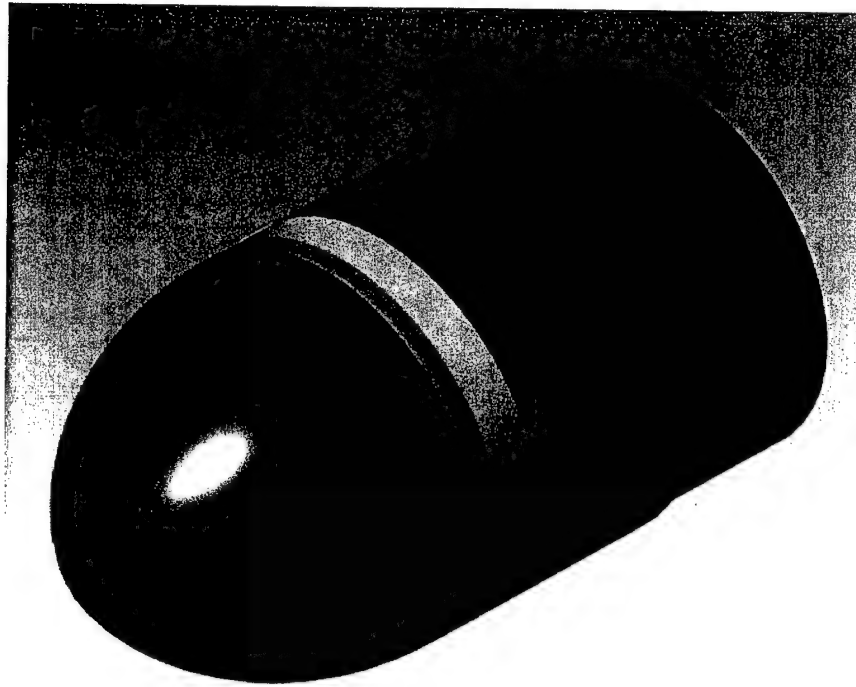


Figure 1. Model of the 40-mm grenade.

grenade when the jet flow is released from various size cavities, at each of the two locations (one on the nose of the projectile and one on the cylinder).

## 2. Solution Technique

The complete set of time-dependent, Reynolds-averaged, thin-layer Navier-Stokes equations is solved numerically to obtain a solution to this problem. The numerical technique used is an implicit, finite difference scheme. Time-accurate calculations are made to numerically simulate a medium-caliber grenade with a jet hole in various locations on the surface of the projectile.

### 2.1 Governing Equations

The complete set of 3-D, time-dependent, generalized-geometry, Reynolds-averaged, thin-layer Navier-Stokes equations is solved numerically to obtain a solution to this problem and can be written in general spatial coordinates  $\xi$ ,  $\eta$ , and  $\zeta$  as follows [4]:

$$\partial_t \hat{q} + \partial_\xi \hat{F} + \partial_\eta \hat{G} + \partial_\zeta \hat{H} = \text{Re}^{-1} \partial_\zeta \hat{S}, \quad (1)$$

where

$\xi = \xi(x, y, z, t)$  – longitudinal coordinate,  
 $\eta = \eta(x, y, z, t)$  – circumferential coordinate,  
 $\zeta = \zeta(x, y, z, t)$  – nearly normal coordinate, and  
 $\tau = t$  – time.

In equation 1,  $\hat{q}$  contains the dependent variables (density, three velocity components, and energy) and  $\hat{F}, \hat{G}$ , and  $\hat{H}$  are flux vectors. The thin-layer approximation is used here, and the viscous terms involving velocity gradients in both the longitudinal and circumferential directions are neglected. The viscous terms are retained in the normal direction,  $\zeta$ , and are collected into the vector  $\hat{S}$ . In the wake or the base region, similar viscous terms [1] are also added in the streamwise direction,  $\xi$ . An implicit, approximately factored scheme is used to solve these equations. For computation of turbulent flows, the turbulent contributions are supplied through an algebraic eddy viscosity turbulence model developed by Baldwin and Lomax [5] or a pointwise turbulence model [6].

## 2.2 Numerical Algorithm

The implicit, approximately factored scheme for the thin-layer Navier-Stokes equations using central differencing in the  $\eta$  and  $\zeta$  directions and upwinding in  $\xi$  is written in the following form [7]:

$$\begin{aligned}
 & \left[ I + i_b h \delta_\xi^b (\hat{A}^+)^n + i_b h \delta_\zeta \hat{C}^n - i_b h \text{Re}^{-1} \bar{\delta}_\zeta J^{-1} \hat{M}^n J - i_b D_i \right]_\zeta \\
 & \times \left[ I + i_b h \delta_\xi^f (\hat{A}^-)^n + i_b h \delta_\eta \hat{B}^n - i_b D_i \right]_\eta \Delta \hat{Q}^n \\
 & = i_b \Delta t \left\{ \delta_\xi^b [(\hat{F}^+)^n - \hat{F}_\infty^-] + \delta_\xi^f [(\hat{F}^-)^n - \hat{F}_\infty^-] + \delta_\eta (\hat{G}^n - \hat{G}_\infty) \right. \\
 & \left. + \delta_\zeta (\hat{H}^n - \hat{H}_\infty) - \text{Re}^{-1} \bar{\delta}_\zeta (\hat{S}^n - \hat{S}_\infty) \right\} - i_b D_e (\hat{Q}^n - \hat{Q}_\infty),
 \end{aligned} \tag{2}$$

where  $h = \Delta t$  or  $(\Delta t)/2$  and the free-stream base solution is used. The free-stream fluxes are subtracted from the governing equation to reduce the possibility of error from the free-stream solution corrupting the converged solution. Here,  $\delta$  is typically a three-point second-order accurate central difference operator,  $\bar{\delta}$  is a midpoint operator used with the viscous terms, and the operators  $\delta_\xi^b$  and  $\delta_\xi^f$

are backward and forward three-point difference operators. The flux  $\hat{F}$  has been eigensplit, and the matrices  $\hat{A}, \hat{B}, \hat{C}$ , and  $\hat{M}$  result from local linearization of the fluxes about the previous time level. Here,  $J$  denotes the Jacobian of the coordinate transformation. Dissipation operators  $D_e$  and  $D_i$  are used in the central space differencing directions. The smoothing terms used in the present study are of the form

$$D_e|_\eta = (\Delta t) J^{-1} \left[ \varepsilon_2 \bar{\delta} \rho(B) \beta \bar{\delta} + \varepsilon_4 \bar{\delta} \frac{\rho(B)}{1 + \beta} \bar{\delta}^3 \right] |_\eta J, \quad (3)$$

and

$$D_i|_\eta = (\Delta t) J^{-1} \left[ \varepsilon_2 \bar{\delta} \rho(B) \beta \bar{\delta} + 2.5 \varepsilon_4 \bar{\delta} \rho(B) \bar{\delta} \right] |_\eta J,$$

where

$$\beta = \frac{|\bar{\delta}^2 P|}{|(1 + \bar{\delta}^2) P|}, \quad (4)$$

and where  $\rho(B)$  is the true spectral radius of  $B$ . The idea here is that the fourth difference will be tuned down near shocks (e.g., as  $\beta$  gets large, the weight on the fourth difference drops down while the second difference tunes up).

### 2.3 Boundary Conditions

For simplicity, most of the boundary conditions have been imposed explicitly. The no-slip boundary condition is used on the grenade surface; it has been modified, however, to allow a jet flow of variable size and location. The pressure at the wall is calculated by solving a combined momentum equation. A symmetry boundary condition is imposed at the circumferential edges of the grid. At the centerline axes, a polar boundary condition is used at the nose of the projectile, while a collapsed axis boundary condition is used at the centerline in back of the projectile. Boundary conditions are not applied at the outer boundary, which is far enough from the body to allow for free stream flow.

---

## 3. Chimera Composite Grid Scheme

---

The chimera overset grid technique [8–10] involves generating independent grids about each component and then oversetting them onto a base grid to form the complete model. This procedure reduces a complex single or multi-body

problem into a number of simpler subproblems. An advantage of the overset grid technique is that it allows computational grids to be obtained for each body component separately and thus makes the grid generation process easier. Because each component grid is generated independently, portions of one grid may lie within a solid boundary contained within another grid. Such points lie outside the computational domain and are excluded from the solution process. Equation 2 has been modified for chimera overset grids by the introduction of the flag  $i_b$  to achieve just that. This  $i_b$  array accommodates the possibility of having arbitrary holes in the grid. The  $i_b$  array is defined so that  $i_b = 1$  at normal grid points and  $i_b = 0$  at hole points. Thus, when  $i_b = 1$ , equation 2 becomes the standard scheme. The set of grid points that forms the border between the hole points and the normal field points is called inter-grid boundary points. These points are updated by interpolating the solution from the overset grid that created the hole. Values of the  $i_b$  array and the interpolation coefficients needed for this update are provided by a separate algorithm [10].

---

#### 4. Model Geometry and Computational Grid

---

The computational model consists of a 40-mm grenade, 1.76 calibers in length. The mesh for this model consists of a single grid, containing approximately 750,000 grid points. Figure 2 shows a cross-sectional view of the longitudinal grid system for this configuration. The grid dimensions are  $151 \times 61 \times 80$  in the longitudinal, circumferential, and normal directions respectively. Initially, the jet holes were modeled by modifying the boundary conditions at specific indices on the surface of the grenade. The jet width is 1.12 mm (0.0281 calibers). In the circumferential direction, the jet was modeled for various size openings:  $6^\circ$  (small),  $45^\circ$  (medium), and  $90^\circ$  (large). In Figures 3 and 4, the jet openings are shaded in black. Figure 3 shows their location on the nose of the grenade. Similar jet holes were also modeled on the cylinder of the grenade at  $X/D = 4.6$  mm (1.49 calibers), as shown in Figure 4. This mesh was used for the steady jet computations. For the jet-off cases, a similar axisymmetric grid was used, with only three planes in the circumferential direction.

For the unsteady jet calculations, the computational mesh for the medium jet was modified to include the jet cavity inside the projectile. The depth of the cavity is 10 mm (0.25 calibers). The original mesh used for the projectile body was refined by increasing the number of points in the axial direction to 187 and by clustering the points in the areas of the nose and cylinder jets. In addition, a small mesh was generated to model the jet cavity inside the projectile body. This mesh consists of approximately 7,000 grid points:  $11 \times 16 \times 41$  in the axial, circumferential, and normal directions. Consequently, the total number of grid points increased to approximately 920,000. Figure 5 shows a computational

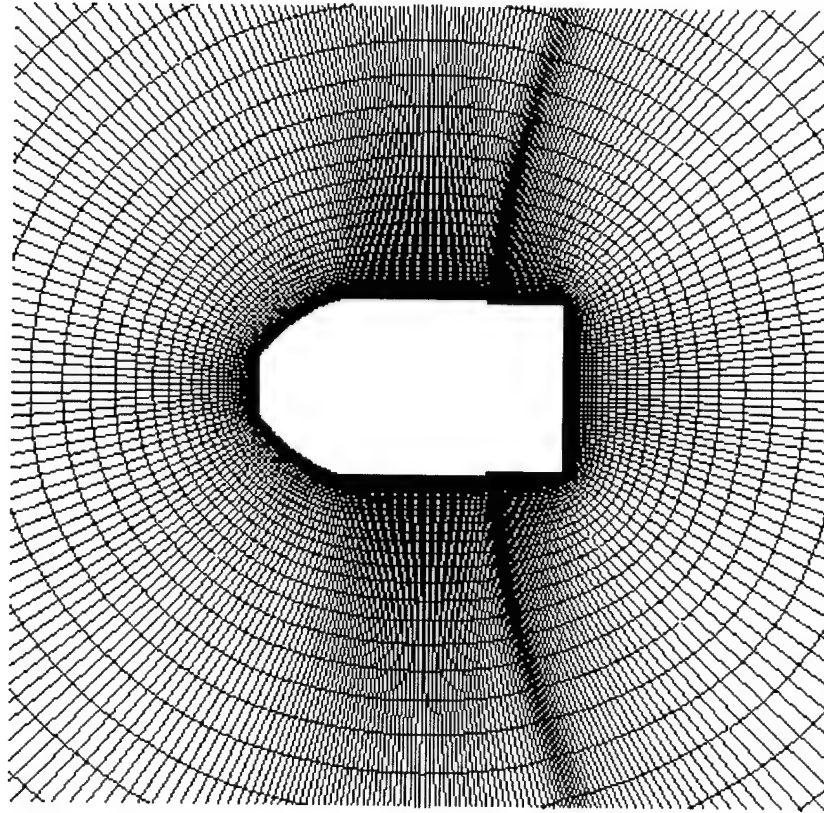


Figure 2. Computational model and grid system.

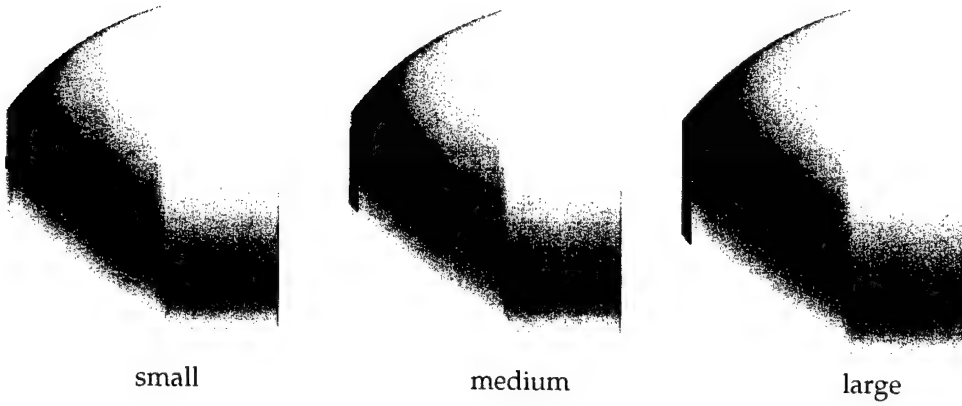


Figure 3. Location of nose jets on the computational model.

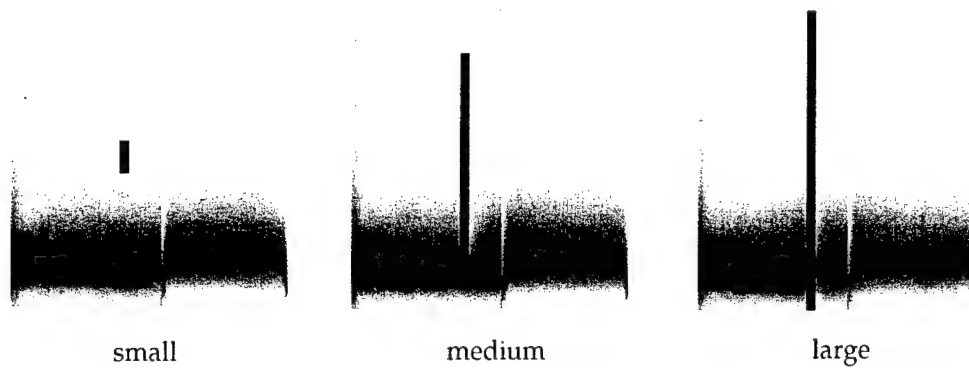


Figure 4. Location of cylinder jets on the computational model.

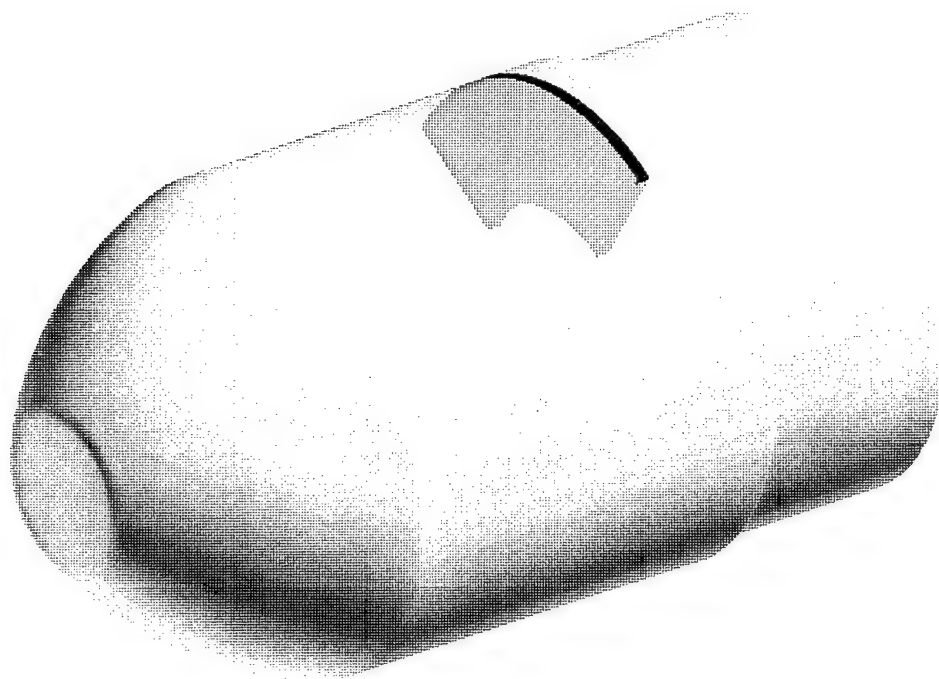


Figure 5. Computational model showing jet cavity.

model of the projectile with the jet cavity. Since the Chimera technique was to be used for the unsteady jet computations, the jet cavity mesh could be moved to various locations if necessary. PEGSUS [11], a mesh interpolation code, was used to provide the necessary intergrid information.

---

## 5. Results

---

CFD computations have provided interesting information about the 40-mm projectile flow field. The results provide insight to the problem and demonstrate the capability of the Zonal Navier-Stokes flow solver ZNSFLOW [12] to provide flow field solutions for a projectile with jets.

### 5.1 Jet-Off

The preliminary effort was to compute axisymmetric solutions at Mach numbers 0.15, 0.2, and 0.25, at  $0^\circ$  angle of attack and wall temperature of  $530^\circ$  Rankin. These calculations required only small amounts of time and memory and were completed on an SGI Onyx system at the U.S. Army Research Laboratory (ARL) Major Shared Resource Center (MSRC) site at Aberdeen Proving Ground, MD. Figure 6 shows the convergence history of the drag force coefficient (CDO) for the jet-off cases. Computed pressure contours for these cases are shown in Figure 7 and show the expected features as the Mach number increases from 0.15 to 0.25 (top to bottom). Figure 8 shows that the change in drag coefficient as a function of Mach number is rather small in the range of Mach numbers considered. As expected, the pressure (wave) drag (CDP) is the largest contributor; the skin friction drag (CDV) component is small. Velocity vectors in the base region, as seen in Figure 9, show the flow to be similar for the computations. Consequently, a Mach number of 0.25 was selected for the jet-on computations.

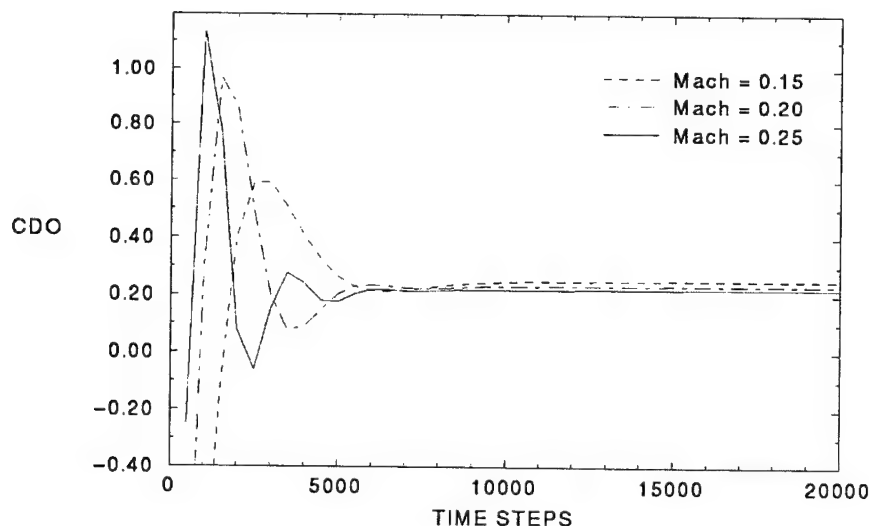


Figure 6. Convergence history, jet-off.

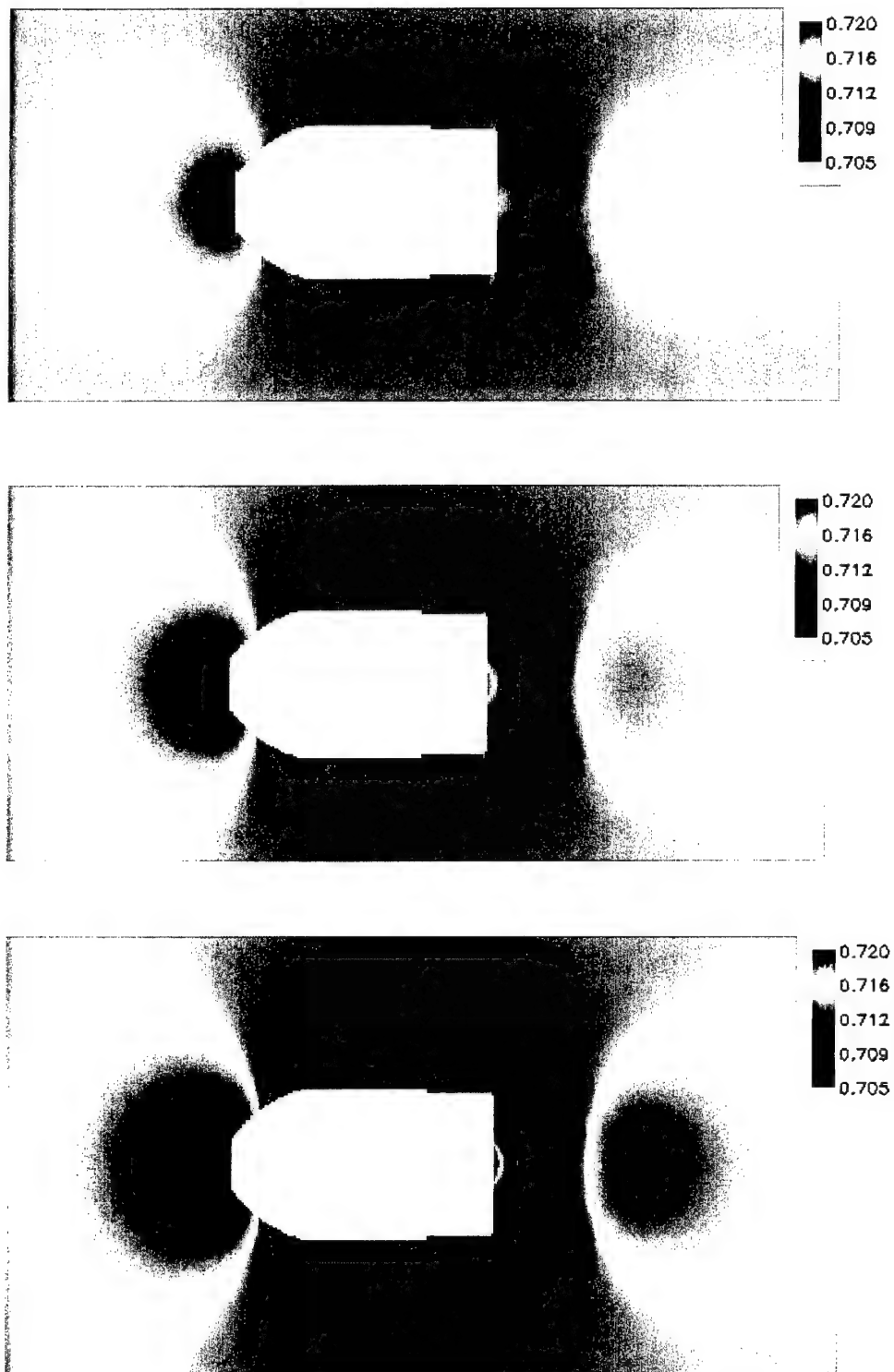


Figure 7. Pressure contours, jet-off; Mach numbers 0.15, 0.2, and 0.25 (top to bottom).

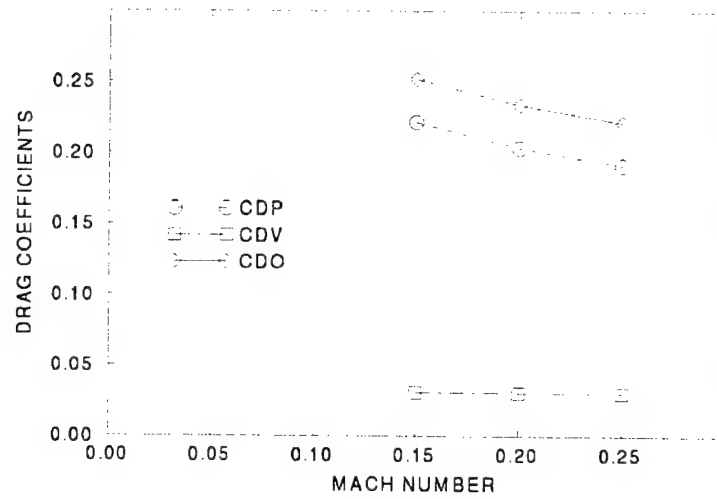


Figure 8. Mach number vs. drag coefficients, jet-off.

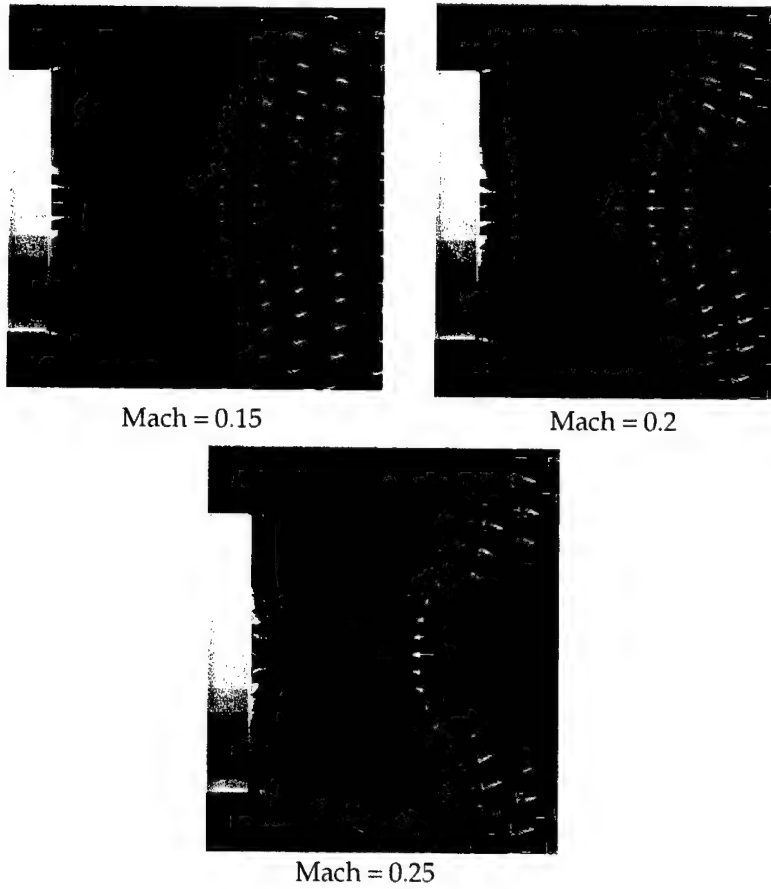


Figure 9. Velocity vectors, base region, jet-off.

## 5.2 Steady Jet

For this study, steady-state numerical computations were performed with the jet on, varying the size and location of the jet holes on a medium size grenade. A jet velocity of Mach 0.125 (one-half the free stream velocity) was used. Computations were completed for a Mach number of 0.25, and at  $0^\circ$  and  $4^\circ$  angles of attack. Sea-level atmospheric flight conditions were used. Each 3-D calculation required approximately 6.6 million words of memory, and each case used an average of 25 hr of computer time on the Silicon Graphics Origin 2000 suite of supercomputers at the ARL MSRC. Resources used for the axisymmetric cases were minimal.

Axisymmetric calculations were done at  $0^\circ$  angle of attack for the nose jet and the cylinder jet. Computational results for the jet-on cases were compared with that of the jet-off case. Figure 10 shows that the nose jet slightly affects the surface pressure distribution on the nose section of the projectile, while the cylinder jet has a stronger effect both upstream and downstream of the jet location. The drag coefficients in Figure 11 show a large decrease due to the nose jet, while the cylinder jet increases drag only slightly. The pressure contours shown in Figure 12 reveal only slight changes in the flow field at the nose of the projectile. The changes are much more dramatic for the cylinder jet and are shown in Figure 13. The differences in the flow field upstream as well as downstream of the jet are clearly visible, especially for the large jet case.

Computed results have been obtained for 3-D steady jet-on cases where a jet was placed either on the nose or the cylinder of the projectile. By specifying indices on the projectile surface, jet flow boundary conditions were provided for jets of three sizes ( $6^\circ$ ,  $45^\circ$ , and  $90^\circ$ ) on the nose of the grenade as well as on the cylindrical section of the projectile (see Figures 3 and 4). A series of computations for the various size jets and locations was performed for both  $0^\circ$  and  $4^\circ$  angle of attack. Surface pressure data was extracted at the  $0^\circ$  plane for all cases. Figure 14 shows a comparison of surface pressure coefficient for all three nose jets. Again the differences are mainly on the nose of the projectile. For the cylinder jets, the differences are quite dramatic, both upstream and downstream of the jet, as seen in Figure 15. A top-side view of surface pressure contours on the body are shown in Figure 16 for the jet-off case and all three cylinder jets. (The jet location is shaded in gray.) The effects of the jet are seen quite clearly. Longitudinal pressure contours of the flow fields shown in Figure 17 also demonstrate this effect.

Force and moment coefficients were computed for all solutions. CN is normal force, CA is axial force (drag), and CMP is the pitching moment. Table 1 contains force and moment data for the nose jet locations and shows that there are only minimal differences for the various size jets. Table 2 shows a slightly stronger difference for the cylinder jet locations, especially for the large jet.

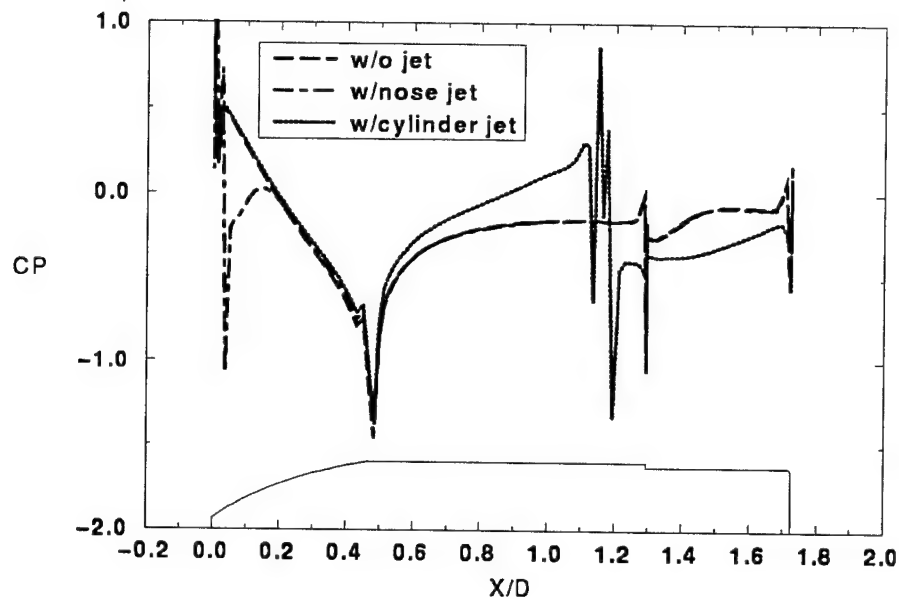


Figure 10. Surface pressure coefficient vs. axial position.

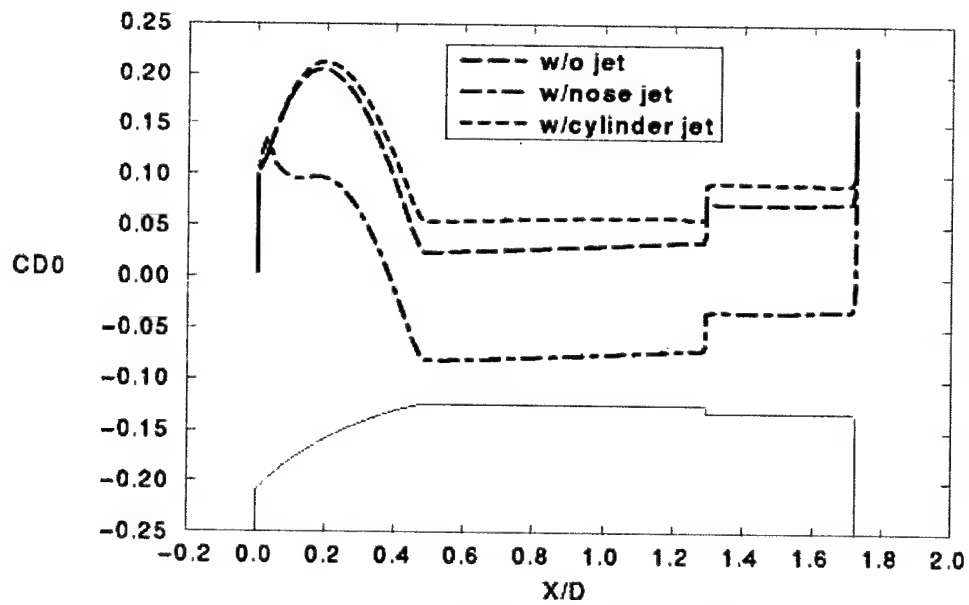


Figure 11. Drag coefficient vs. axial position.

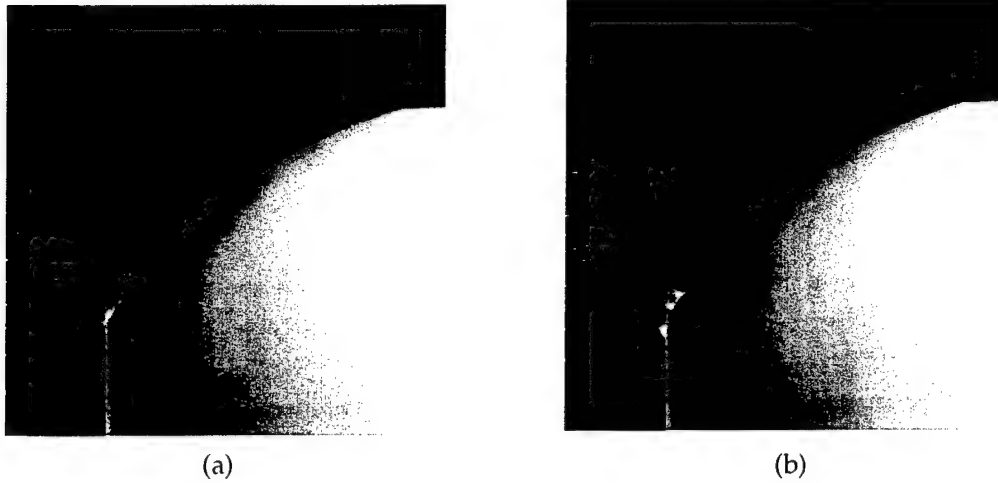


Figure 12. Pressure contours in nose area, (a) jet-off and (b) jet-on.



Figure 13. Pressure contours in cylinder area, (a) jet-off and (b) jet-on.

### 5.3 Unsteady Jet

For computational validation of the unsteady jet CFD modeling, an isolated two-dimensional (2-D) case was first selected. A schematic diagram and a flow picture obtained from the experiment for this isolated 2-D jet are shown in Figure 18. Here the jet width is 0.5 mm and the peak jet velocity is 20 m/s. In the experiment, the synthetic jet was formed in air at an orifice measuring 0.5 mm (width)  $\times$  75 mm (length). The jet actuator operates at a frequency of 1,000 Hz [13]. The jet is synthesized by the time-harmonic motion of a flexible diaphragm in a sealed cavity. This motion results in both positive and negative velocities at the jet exit while the net mass flux out of the cavity is zero during each cycle. In the computations, unsteady jet boundary conditions were applied

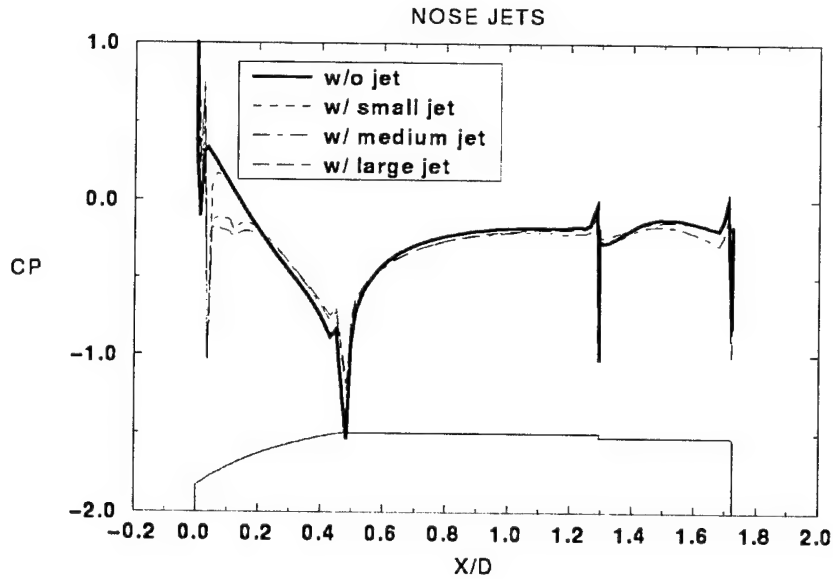


Figure 14. Surface pressure coefficient—nose jets.

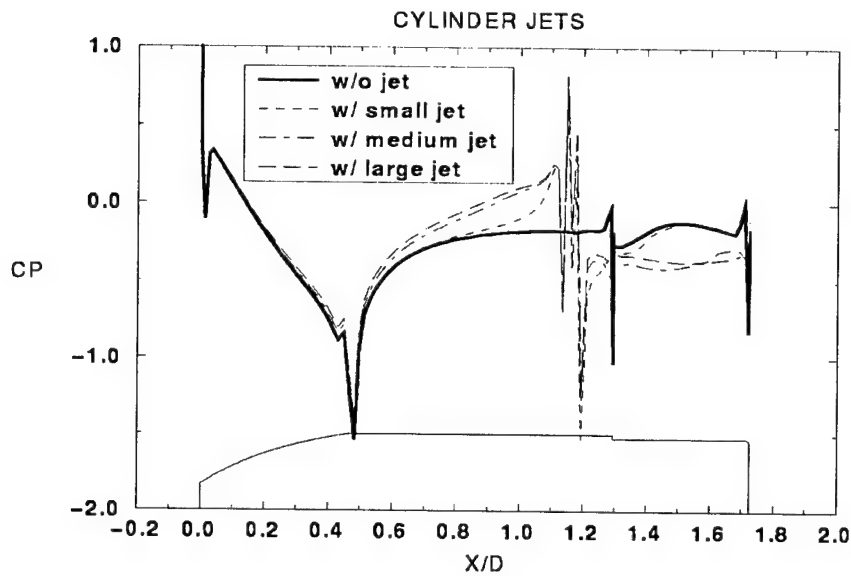


Figure 15. Surface pressure coefficient—cylinder jets.

with a sinusoidal variation in the jet velocity with a peak amplitude of 20 m/s. Computed velocity and vorticity contours are shown in Figure 19. The time-averaged jet centerline velocity over many cycles of unsteady jet CFD computations is compared with available time-averaged experimental data in Figure 20 and is found to be in reasonable agreement. As shown both in the

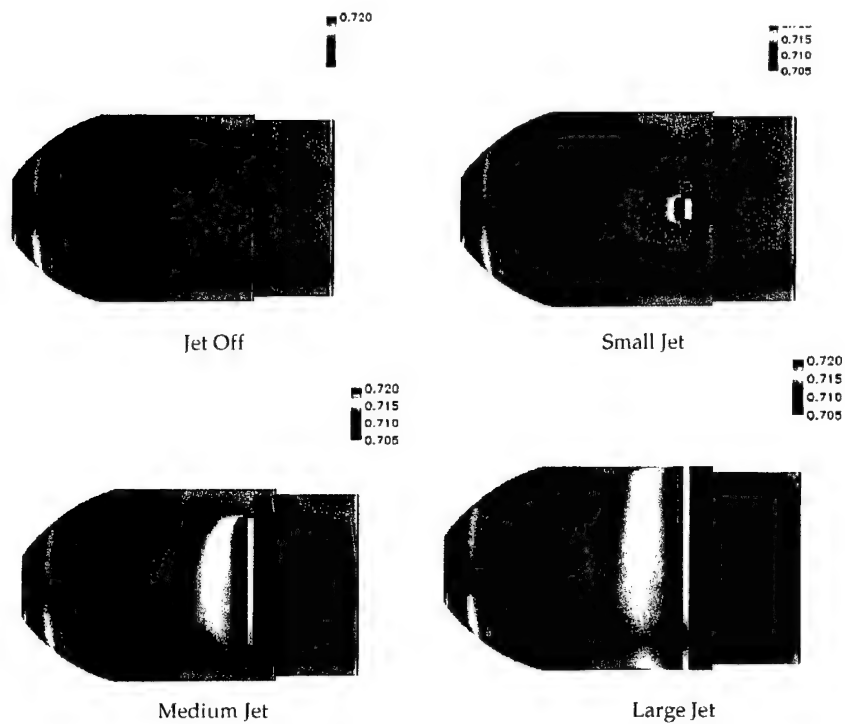


Figure 16. Surface pressure contours—cylinder jets.

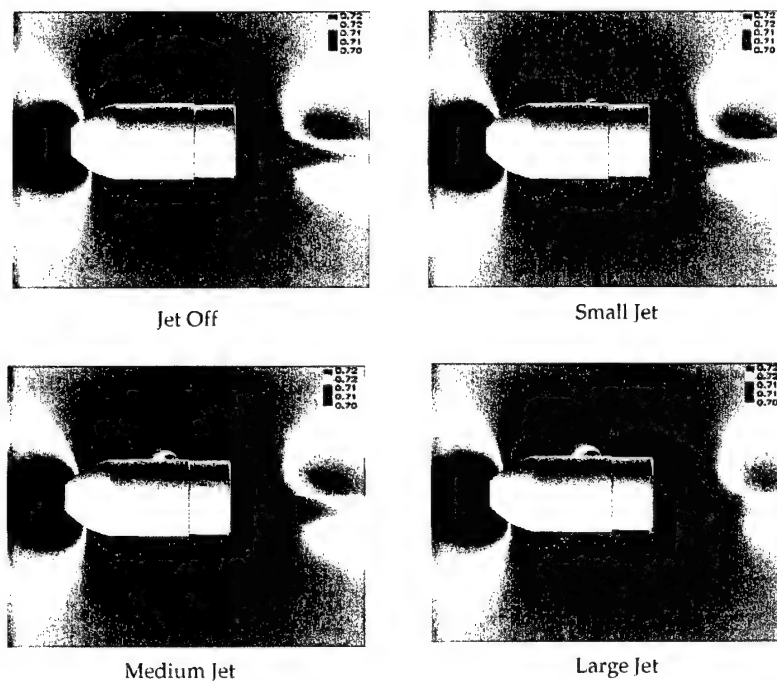


Figure 17. Pressure contours, cylinder jets, longitudinal view.

Table 1. Force and moment coefficients for nose jets,  $\alpha = 4$ .

	No Jet	Small Jet	Medium Jet	Large Jet
CN	0.161	0.160	0.166	0.163
CA	0.276	0.276	0.25	0.221
CMP	-0.109	-0.106	-0.11	-0.11

Table 2. Force and moment coefficients for cylinder jets,  $\alpha = 4$ .

	No Jet	Small Jet	Medium Jet	Large Jet
CN	0.161	0.161	0.166	0.129
CA	0.276	0.279	0.267	0.244
CMP	-0.109	-0.114	-0.172	-0.156

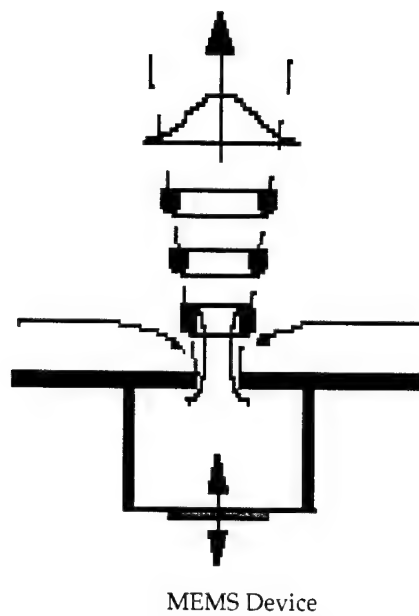


Figure 18. Schematic and flow picture of a 2-D jet experiment.

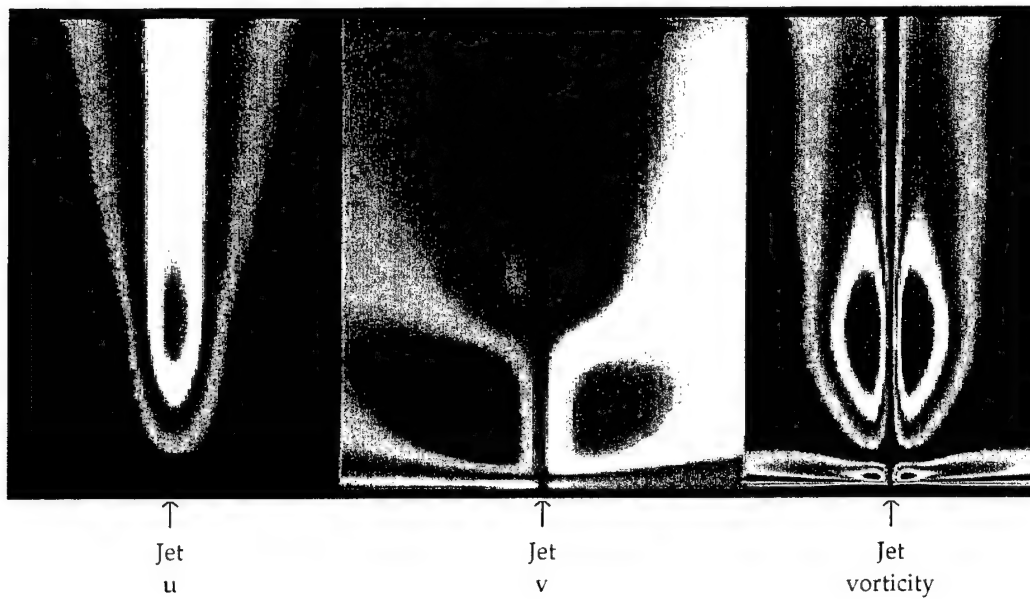


Figure 19. Velocity components  $u$ ,  $v$ , and vorticity for an unsteady jet.

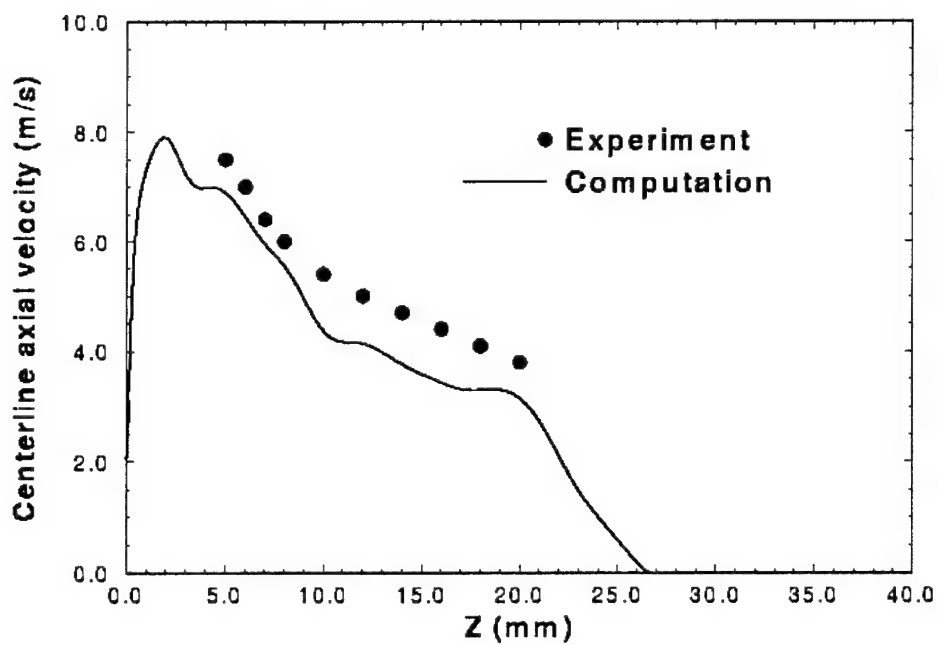


Figure 20. Variation of time-averaged centerline jet velocity with distance from the wall, unsteady jet.

experiment and the computations, the time-averaged centerline velocity is decreased with increasing distance away from the jet exit. The next step was to apply similar unsteady jet boundary conditions to the subsonic projectile case. For this case, the jet cavity inside the projectile was included (see Figure 5). The unsteady jet boundary conditions were applied at the bottom wall of the jet cavity. Numerical results were obtained for this unsteady jet case at  $Mach = 0.25$  and zero angle of attack. The jet width was 2.24 mm and the peak jet velocity used was 43 m/s operating at a frequency of 1,000 Hz. Computed surface pressures obtained at a given instant in time are shown in Figure 21. It also shows particle traces coming out of the cavity. The pressure field both upstream and downstream of the jet is affected by the jet flow depending on whether the flow is into or out of the cavity. Additional qualitative features of the flow field are shown in Figure 22. This figure shows the snapshots of the computed velocity vectors in the vicinity of the jet exit at two different instants in time. Figure 22(a) clearly shows the external free stream flow going into the jet cavity whereas Figure 22(b) shows the flow coming out of the cavity and interacting with the free stream flow. Figure 22(b) also shows a region of separated flow just downstream of the jet exit. The resulting surface pressures are integrated to obtain the aerodynamic forces and moments. The computed axial force, the normal force, and the pitching moment coefficients are shown in Figure 23 as a function of time for a cycle. These results clearly indicate the unsteady nature of the flow. Similar results were obtained for this projectile at an angle of attack of  $4^\circ$  (see Figure 24). These results are being analyzed to determine the feasibility of these jets to provide control authority. It is anticipated that multiple jets may be required to provide the control authority needed for maneuvering a subsonic projectile.

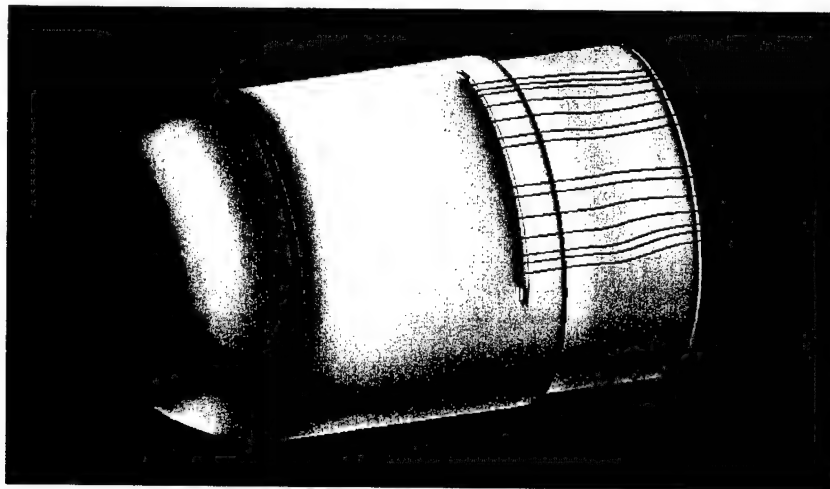


Figure 21. Computed surface pressures,  $M = 0.25$ ,  $\alpha = 0$ , unsteady jet.

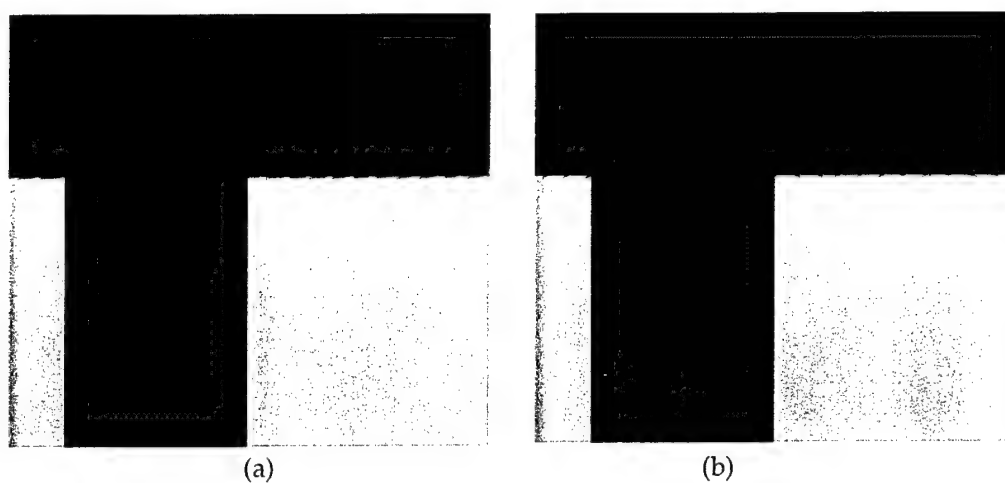


Figure 22. Velocity vectors at two instants in time during the cycle,  $M = 0.25$ ,  $\alpha = 0$ , unsteady jet.

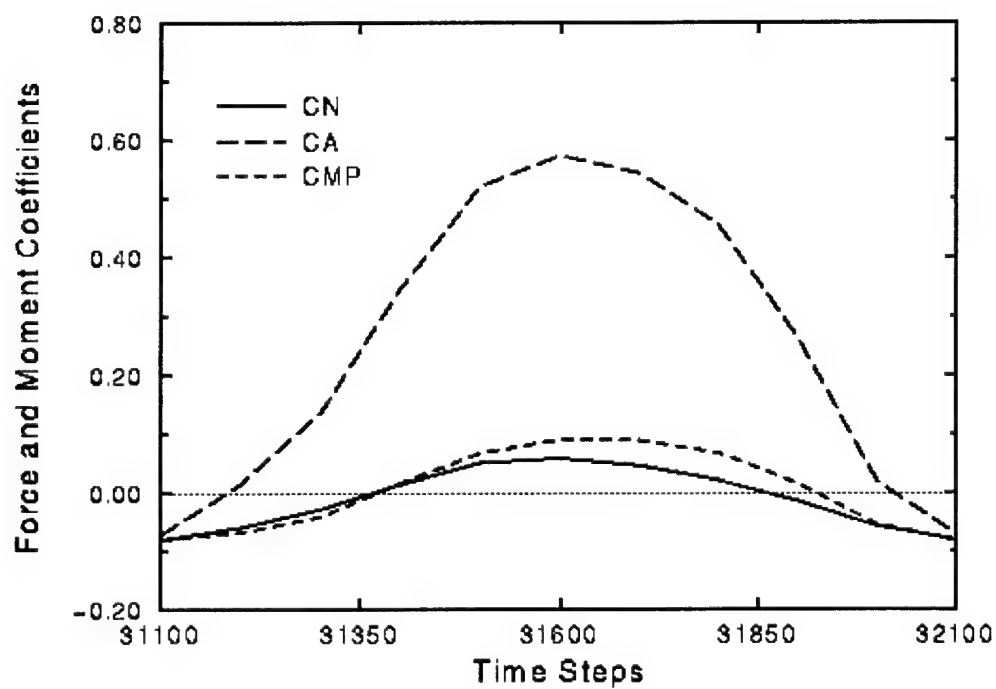


Figure 23. Force and moment coefficients,  $M = 0.25$ ,  $\alpha = 0$ , unsteady jet.

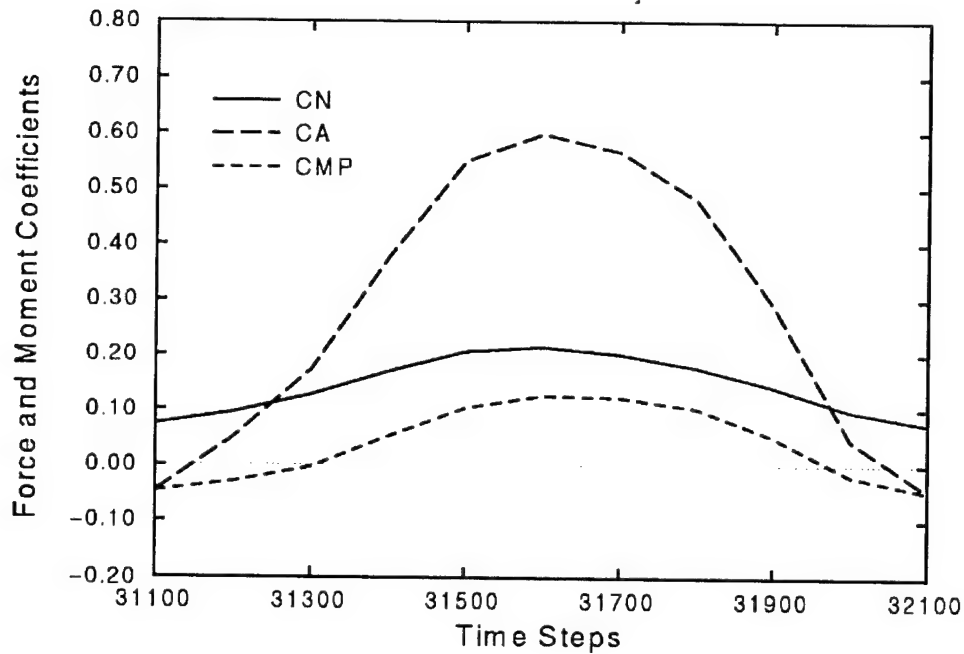


Figure 24. Force and moment coefficients,  $M = 0.25$ ,  $\alpha = 0$ , unsteady jet.

## 6. Conclusion

A computational study has been undertaken to consider the aerodynamic effect of small tiny jets as a means to provide the control authority needed to maneuver a projectile at low subsonic speeds. Computed results have been obtained at subsonic speeds and at  $0^\circ$  and  $4^\circ$  angle of attack. Both steady and unsteady jets have been simulated. Qualitative flow field features show the interaction of tiny jets and the extent of their influence both upstream and downstream of the jet. The CFD results also show the effect of the jet locations and sizes on the surface pressure distribution. The unsteady jet results obtained for a 2-D jet are compared with the experimental data and are found to be in reasonable agreement. The unsteady jet has been applied to the subsonic projectile and is shown to have some effect on forces and moments even at zero degree angle of attack. The results show the potential of CFD to provide insight into the jet interaction flow fields and provide guidance as to the locations and sizes of the jets to generate the maximum control authority for maneuvering smart munitions.

---

## 7. References

---

1. Sahu, J., K. R. Heavey, and E. N. Ferry. "Computational Fluid Dynamics for Multiple Projectile Configurations." Proceedings of the 3rd Overset Composite Grid and Solution Technology Symposium, Los Alamos, NM, October 1996.
2. Sahu, J., K. R. Heavey, and C. J. Nietubicz. "Time-Dependent Navier-Stokes Computations for Submunitions in Relative Motion." Proceedings of the 6th International Symposium on Computational Fluid Dynamics, Lake Tahoe, NV, September 1995.
3. Sahu, J., H. L. Edge, K. R. Heavey, and E. N. Ferry. "Computational Fluid Dynamics Modeling of Multi-body Missile Aerodynamic Interference." ARL-TR-1765, U.S. Army Research Laboratory, Aberdeen Proving Ground, MD, August 1998.
4. Pulliam, T. H., and J. L. Steger. "On Implicit Finite Difference Simulations of Three-Dimensional Flow." *AIAA Journal*, vol. 18, no. 2, pp. 167-169, February 1982.
5. Baldwin, B. L., and H. Lomax. "Thin Layer Approximation and Algebraic Model for Separated Turbulent Flows." AIAA 78-257, American Institute of Aeronautics and Astronautics, Reston, VA, January 1978.
6. Goldberg, U. C., O. Perroomian, and S. Chakravarthy. "A Wall-Distance Free K-E Model With Enhanced Near-Wall Treatment." *ASME Journal of Fluids Engineering*, vol. 120, pp. 457-462, 1998.
7. Steger, J. L., S. X. Ying, and L. B. Schiff. "A Partially Flux-Split Algorithm for Numerical Simulation of Compressible Inviscid and Viscous Flows." Proceedings for the Workshop on Computational Fluid Dynamics, Institute of Non-Linear Sciences, University of California, Davis, CA, 1986.
8. Steger, J. L., F. C. Dougherty, and J. A. Benek. "A Chimera Grid Scheme." *Advances in Grid Generation*, ASME FED-5, edited by K. N. Ghia and U. Ghia, June 1983.
9. Benek, J. A., T. L. Donegan, and N. E. Suhs. "Extended Chimera Grid Embedding Scheme With Application to Viscous Flows." AIAA 87-1126-CP, American Institute of Aeronautics and Astronautics, Reston, VA, 1987.
10. Meakin, R. L. "Computations of the Unsteady Flow About a Generic Wing/Pylon/Finned-Store Configuration." AIAA 92-4568-CP, American Institute of Aeronautics and Astronautics, Reston, VA, August 1992.

11. Suhs, N. E., and R. W. Tramel. "PEGSUS 4.0 User's Manual." AEDC-TR-8, Arnold Engineering Development Center, Arnold, TN, November 1991.
12. Edge, H. L., J. Sahu, W. B. Sturek, D. M. Pressel, K. R. Heavey, P. Weinacht, C. K. Zoltani, C. J. Nietubicz, J. Clarke, M. Behr, and P. Collins. "Common High Performance Computing Software Support Initiative (CHSSI) Computational Fluid Dynamics CFD-6 Project Final Report: ARL Block-Structured Gridding Zonal Navier-Stokes Flow (ZNSFLOW) Solver Software." ARL-TR-2084, U.S. Army Research Laboratory, Aberdeen Proving Ground, MD, February 2000.
13. Smith, B. B., and A. Glezerz. "The Formation and Evolution of Synthetic Jets." *Journal of Physics of Fluids*, vol. 10, no. 9, September 1998.

NO. OF  
COPIES ORGANIZATION

2 DEFENSE TECHNICAL  
INFORMATION CENTER  
DTIC OCA  
8725 JOHN J KINGMAN RD  
STE 0944  
FT BELVOIR VA 22060-6218

1 HQDA  
DAMO FDT  
400 ARMY PENTAGON  
WASHINGTON DC 20310-0460

1 OSD  
OUSD(A&T)/ODDR&E(R)  
DR R J TREW  
3800 DEFENSE PENTAGON  
WASHINGTON DC 20301-3800

1 COMMANDING GENERAL  
US ARMY MATERIEL CMD  
AMCRDA TF  
5001 EISENHOWER AVE  
ALEXANDRIA VA 22333-0001

1 INST FOR ADVNCD TCHNLGY  
THE UNIV OF TEXAS AT AUSTIN  
3925 W BRAKER LN STE 400  
AUSTIN TX 78759-5316

1 US MILITARY ACADEMY  
MATH SCI CTR EXCELLENCE  
MADN MATH  
THAYER HALL  
WEST POINT NY 10996-1786

1 DIRECTOR  
US ARMY RESEARCH LAB  
AMSRL D  
DR D SMITH  
2800 POWDER MILL RD  
ADELPHI MD 20783-1197

1 DIRECTOR  
US ARMY RESEARCH LAB  
AMSRL CI AI R  
2800 POWDER MILL RD  
ADELPHI MD 20783-1197

NO. OF  
COPIES ORGANIZATION

3 DIRECTOR  
US ARMY RESEARCH LAB  
AMSRL CI LL  
2800 POWDER MILL RD  
ADELPHI MD 20783-1197

3 DIRECTOR  
US ARMY RESEARCH LAB  
AMSRL CI IS T  
2800 POWDER MILL RD  
ADELPHI MD 20783-1197

ABERDEEN PROVING GROUND

2 DIR USARL  
AMSRL CI LP (BLDG 305)

NO. OF  
COPIES ORGANIZATION

2 USAF WRIGHT AERONAUTICAL  
LABORATORIES  
AFWAL FIMG  
J SHANG  
N E SCAGGS  
WPAFB OH 45433-6553

1 CDR NSWC  
W YANTA CODE B40  
DAHLGREN VA 22448-5100

1 CDR NSWC  
A WARDLAW CODE 420  
INDIAN HEAD MD 20640-5035

4 DIR NASA  
LANGLEY RESRCH CTR  
TECH LIBRARY  
D M BUSHNELL  
M J HEMSCH  
J SOUTH  
LANGLEY STATION  
HAMPTON VA 23665

2 ARPA  
P KEMMEY  
J RICHARDSON  
3701 N FAIRFAX DR  
ARLINGTON VA 22203-1714

6 DIR NASA  
AMES RSRCH CTR  
T HOLST MS 258 1  
D CHAUSSEE MS 258 1  
M RAI MS 258 1  
P KUTLER MS 258 1  
P BUNING MS 258 1  
B MEAKIN MS 258 1  
MOFFETT FIELD CA 94035

1 DIR NASA  
AMES RSRCH CTR  
L SCHIFF MS 227 8  
MOFFETT FIELD CA 94035

1 USMA  
DEPT OF MECHANICS  
LTC A L DULL  
WEST POINT NY 10996

NO. OF  
COPIES ORGANIZATION

1 CDR  
US ARMY TACOM ARDEC  
AMSTA AR FSF T  
BLDG 382  
C NG  
PICATINNY ARSENAL NJ  
07806-5000

1 CDR  
US ARMY TACOM ARDEC  
AMSTA AR FSF T  
BLDG 382  
H HUDGINS  
PICATINNY ARSENAL NJ  
07806-5000

1 CDR  
US ARMY TACOM ARDEC  
AMSTA AR FSF T  
BLDG 382  
J GRAU  
PICATINNY ARSENAL NJ  
07806-5000

1 CDR  
US ARMY TACOM ARDEC  
AMSTA AR FSF T  
BLDG 382  
W KOENIG  
PICATINNY ARSENAL NJ  
07806-5000

1 CDR  
US ARMY TACOM  
AMSTA AR CCH B  
P VALENTI  
BLDG 65 S  
PICATINNY ARSENAL NJ  
07806-5001

1 CDR  
US ARMY ARDEC  
SFAE FAS SD  
M DEVINE  
PICATINNY ARSENAL NJ  
07806-5001

1 CDR  
US NAVAL SURFACE  
WEAPONS CTR  
F MOORE  
DAHLGREN VA 22448

NO. OF  
COPIES   ORGANIZATION

2   UC DAVIS  
DEPT OF MECHL ENGRG  
H A DWYER  
M HAFEZ  
DAVIS CA 95616

1   AEROJET ELECT PLANT  
D W PILLASCH  
B170 DEPT 5311  
P O BOX 296  
1100 W HOLLYVALE ST  
AZUSA CA 91702

3   AIR FORCE ARMAMENT LAB  
AFATL FXA  
S C KORN  
B SIMPSON  
D BELK  
EGLIN AFB FL 32542-5434

1   MIT  
TECH LIBRARY  
77 MASSACHUSETTS AVE  
CAMBRIDGE MA 02139

1   GRUMMAN AEROSPACE CORP  
AEROPHYSICS RSRCH DEPT  
R E MELNIK  
BETHPAGE NY 11714

2   MICRO CRAFT INC  
J BENEK  
N SUHS  
207 BIG SPRINGS AVE  
TULLAHOMA TN 37388-0370

1   LOS ALAMOS NATL LAB  
B HOGAN  
MS G770  
LOS ALAMOS NM 87545

2   DIR  
SANDIA NATL LABS  
W OBERKAMPF DIV 1554  
F BLOTTNER DIV 1554  
ALBUQUERQUE NM 87185

1   DIR  
SANDIA NATL LABS  
W WOLFE DIV 1636  
ALBUQUERQUE NM 87185

NO. OF  
COPIES   ORGANIZATION

1   NAWC  
D FINDLAY  
MS 3 BLDG 2187  
PATUXENT RIVER MD 20670

1   METACOMP TECH INC  
S R CHAKRAVARTHY  
650 HAMPSHIRE ROAD  
SUITE 200  
WESTLAKE VILLAGE CA  
91361-2510

2   ROCKWELL SCIENCE CTR  
V RAMAKRISHNAN  
V V SHANKAR  
1049 CAMINO DOS RIOS  
THOUSAND OAKS CA 91360

1   ADVANCED TECH CTR  
ARVIN CALSPAN  
AERODYNAMICS RSRCH DEPT  
M S HOLDEN  
PO BOX 400  
BUFFALO NY 14225

1   PENN STATE UNIV  
DEPT OF AEROSPACE ENGRG  
G S DULIKRAVICH  
UNIVERSITY PARK PA 16802

1   UIUC  
DEPT OF MECHL AND  
INDUSTRIAL ENGRG  
J C DUTTON  
URBANA IL 61801

1   UNIV OF MARYLAND  
DEPT OF AEROSPACE ENGRG  
J D ANDERSON JR  
COLLEGE PARK MD 20742

1   UNIV OF NOTRE DAME  
DEPT OF AERONAUTICAL  
AND MECHL ENGRG  
T J MUELLER  
NOTRE DAME IN 46556

1   UNIVERSITY OF TEXAS  
DEPT OF AEROSPACE ENG MECH  
D S DOLLING  
AUSTIN TX 78712-1055

<u>NO. OF COPIES</u>	<u>ORGANIZATION</u>
1	UNIV OF DELAWARE DEPT OF MECHL ENGRG J MEAKIN NEWARK DE 19716
1	CDR USAAMCOM AMSAM RD SS G LANDINGHAM REDSTONE ARSENAL AL 35898-5252
3	CDR USAAMCOM AMSAM RD SS AS E KREEGER C D MIKKELSON E VAUGHN REDSTONE ARSENAL AL 35898-5252
1	CDR US ARMY TACOM ARDEC BLDG 162S AMCPM DS MO P J BURKE PICATINNY ARSENAL NJ 07806-5000

<u>NO. OF COPIES</u>	<u>ORGANIZATION</u>
	<u>ABERDEEN PROVING GROUND</u>
3	CDR US ARMY ARDEC FIRING TABLES BRANCH R LIESKE R EITMILLER F MIRABELLE BLDG 120 APG MD 21005
24	DIR USARL AMSRL CI C NIETUBICZ W STUREK AMSRL WM J H SMITH AMSRL WM B A W HORST JR W CIEPIELA AMSRL WM BA D LYON T BROWN AMSRL WM BC P PLOSTINS M BUNDY G COOPER J DESPIRITO J GARNER B GUIDOS K HEAVEY V OSKAY J SAHU K SOENCKSEN P WEINACHT S WILKERSON A ZIELINSKI AMSRL WM BD B FORCH M NUSCA AMSRL WM BF J LACETERA H EDGE AMSRL SL BE A MIKHAIL

REPORT DOCUMENTATION PAGE			Form Approved OMB No. 0704-0188	
Public reporting burden for this collection of information is estimated to average 1 hour per response, including the time for reviewing instructions, searching existing data sources, gathering and maintaining the data needed, and completing and reviewing the collection of information. Send comments regarding this burden estimate or any other aspect of this collection of information, including suggestions for reducing this burden, to Washington Headquarters Services, Directorate for Information Operations and Reports, 1215 Jefferson Davis Highway, Suite 1204, Arlington, VA 22202-4302, and to the Office of Management and Budget, Paperwork Reduction Project(0704-0188), Washington, DC 20503.				
1. AGENCY USE ONLY (Leave blank)		2. REPORT DATE September 2001		3. REPORT TYPE AND DATES COVERED Final, February 1999-March 2001
4. TITLE AND SUBTITLE Computational Fluid Dynamics Modeling of a 40-mm Grenade With and Without Jet Flow			5. FUNDING NUMBERS 1L1612618AH80	
6. AUTHOR(S) Jubaraj Sahu and Karen R. Heavey				
7. PERFORMING ORGANIZATION NAME(S) AND ADDRESS(ES) U.S. Army Research Laboratory ATTN: AMSRL-WM-BC Aberdeen Proving Ground, MD 21005-5066			8. PERFORMING ORGANIZATION REPORT NUMBER ARL-TR-2572	
9. SPONSORING/MONITORING AGENCY NAMES(S) AND ADDRESS(ES)			10. SPONSORING/MONITORING AGENCY REPORT NUMBER	
11. SUPPLEMENTARY NOTES				
12a. DISTRIBUTION/AVAILABILITY STATEMENT Approved for public release; distribution is unlimited.			12b. DISTRIBUTION CODE	
13. ABSTRACT (Maximum 200 words)  This report describes a computational study undertaken to consider the aerodynamic effect of small tiny jets as a means to provide the control authority needed to maneuver a projectile at low subsonic speeds. Scalable Navier-Stokes computational techniques have been used to obtain numerical solutions for the jet-interaction flow field for a projectile at subsonic speeds. Computed results have been obtained at low subsonic speeds at 0° and 4° angle of attack. Both steady and unsteady jets have been considered. For comparison purposes, a jet-off case was also computed. Qualitative flow field features show the interaction of jets with the free stream flow. Numerical results show the effect of the jet locations and sizes on the flow field and surface pressures, and hence on the aerodynamic coefficients. Unsteady jet results have been obtained for a two-dimensional (2-D) jet flow and compared with experimental data for validation. Some results obtained with an unsteady jet for the subsonic projectile are included. These numerical results are being assessed to determine if small tiny jets can be used to provide the control authority needed for maneuvering munitions in lieu of canards and fins.				
14. SUBJECT TERMS Computational fluid dynamics, jet interaction, subsonic flow, numerical simulations, projectile aerodynamics			15. NUMBER OF PAGES 32	
			16. PRICE CODE	
17. SECURITY CLASSIFICATION OF REPORT UNCLASSIFIED	18. SECURITY CLASSIFICATION OF THIS PAGE UNCLASSIFIED	19. SECURITY CLASSIFICATION OF ABSTRACT UNCLASSIFIED	20. LIMITATION OF ABSTRACT UL	

INTENTIONALLY LEFT BLANK.